Exp. Theo. NANOTECHNOLOGY 10 (2026) 357-371 https://doi.org/10.56053/10.S.357

Ultraviolet-visible spectra of pyrromethene 580 laser dye utilizing density functional theory: Examination of molecular structure, electronic characteristics

Saif B. Mohammed[1], Asal A. Mohammed[2], Qudama Kh. Hammad [3,], Omar S. Shawki[1], Falah A-H. Mutlak[4,*], Adil N. Ayyash[5]*

[1]Anbar University, Nanomaterials Research Center, Ramadi, Iraq
[2]College of Energy and Environmental Sciences, Al-Karkh University of Science, Baghdad, Iraq
[3]Al Ma'moun University College, Department of Medical Physics, Baghdad, Iraq
[4]University of Baghdad, College of Science Department of Physics, Baghdad, Iraq
[5] Anbar University, Department of Physics, College of Science, Anbar, Iraq
[*]) Email: qudama.k@almamonuc.edu.iq

Received 17/11/2025, *Received in revised form* 15/12/2025, *Accepted* 28/12/2025, *Published* 15/2/2026

This study presents a theoretical simulation of the pyrromethene 580 molecule using density functional theory (DFT) with the B3LYP functional and a 6-31G (d,p) basis set. DFT methods are employed to determine bond lengths and angles, as well as electronic properties, including electronic energy, dipole moment, electron affinity, ionization potential, chemical Potential, absolute hardness, perfect softness, and electrophilicity index (ω). Additionally, the molecular electrostatic potential and absorption spectra are analyzed. The computed energy value is -1192.534269 Hartree. The dipole moment is found to be 3.96 Debye, indicating a non-uniform charge distribution. The energy gap is calculated as 2.96 eV, reflecting the molecule's stability, while the maximum absorption wavelength (λmax) is 515 nm.

Keywords: DFT; Ionization; UV.

1. INTRODUCTION

At the nanoscale, the electronic structure of functional materials becomes highly sensitive to quantum confinement and charge distribution, making first-principles calculations essential for accurate interpretation. Density Functional Theory (DFT) and Time-Dependent DFT (TD-DFT) provide a robust framework for predicting ionization potential, electronic transitions, and optical response, enabling a

reliable correlation between nanoscale structure and spectroscopic behavior. Pyrromethenes (PMs), or Boron-dipyrromethene (BODIPY) dyes, constitute a highly effective class of laser dyes used in various laser applications [1]. These dyes comprise dipyrromethene complicated with disubstituted boron molecules, often a BF_2 unit, and possess a boron-dipyrromethene tricyclic ring system at their center. BODIPYs are adjustable in the green-yellow segment of the visible spectrum. They are distinguished by excellent lasing efficiency, exceptional photostability, substantial fluorescent quantity, a fixed low intersystem crossing rate, and a high molar absorption factor. Their excitation and emission peaks are prominent; however, their Stokes shift is relatively small, and they may be affected by dye-dye quenching effects and environmental factors that alter their brightness. [2,3]The photophysical characteristics of BODIPY dyes can be modified by introducing appropriate substitutions in the molecular structure of the parent chromophore. Specific BODIPY complexes are available for purchase. The 1,3,5,7,8-pentamethyl-2,6-diethyl-BODIPY complex, known as Pyromethene-567 (PM 567), exhibits lasing at 547 nm. The chemical compound Pyromethene-580 (PM 580) consists of 1,3,5,7,8-pentamethyl-2,6-din-butylpyrromethene-difluoroborate and has the formula C22H33BF2N2 (Figure 1) [4]. Multiple studies have shown that Density Functional Theory (DFT) methods can precisely calculate these dyes' molecular configurations and vibrational frequencies. (DFT) has emerged as the predominant technique for ascertaining electrical ground state structures in quantum chemistry and solid-state physics. It provides an improved equilibrium between precision and computing efficiency relative to alternative ab initio approaches [5,6]. Theoretical modeling and advanced physicochemical analysis have become essential tools for understanding the electronic structure and stability of functional materials. Previous studies have demonstrated that a detailed evaluation of charge distribution, energy gap, and redox-related parameters provides valuable insight into molecular stability and electronic behavior under external perturbations [7].

Previous studies have shown that modifying nanomaterial composition can significantly influence optical absorption behavior and electronic transitions, leading to measurable changes in the optical energy gap and refractive-related parameters. In particular, UV–Vis analysis has proven effective in correlating compositional variation with band gap tuning and electronic structure evolution in functional materials [8].

In addition, systematic analysis of energetic states and electronic transitions has proven effective in correlating molecular structure with observable spectroscopic properties, offering a robust framework for interpreting UV–Vis absorption features in complex systems [9]. This study utilizes experimental results and computational (theoretical) methods to examine the configuration, electronic characteristics, and electronic spectrum of (PM-580) in methanol solutions through the TDDFT methodology.

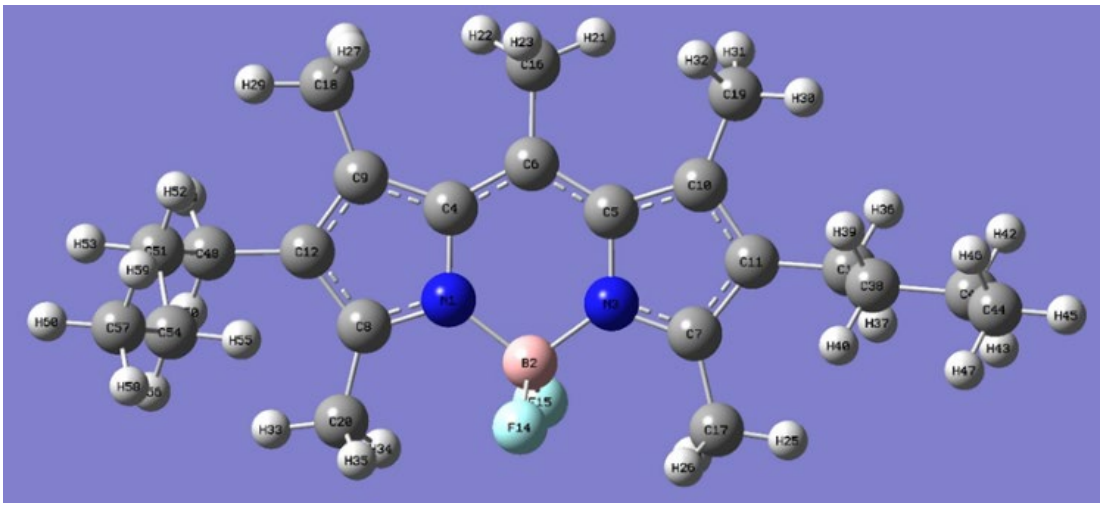

Figure 1 Optimized geometric structure of the bond length PM580 by B3LYP.

2. EXPERIMENTAL

The Pyrromethene 580 (PM-580) dye laser, sourced from British Drug Houses (BDH) and Sigma-Aldrich, possesses a molecular mass of 374.32 g/mol and a molecular formula of C22H33BF2N2. This research highlights the utilization of DFT (Density Functional Theory) and TDDFT (Time-Dependent Density Functional Theory) for PM-580 580. All computational evaluations are conducted utilizing DFT and TDDFT methodologies at the B3LYP/6-31G(d,p) theoretical level. Calculations are performed utilizing Gaussian 09 software and the Gauss View Software for molecular visualization on a personal computer [10]. Seven. The gradient-corrected B3LYP functionality in DFT is very proficient at determining ground-state geometrical and electronic characteristics.

Time-Dependent Density Functional Theory (TD-DFT) techniques at the B3LYP/6-31G(d,p) level are used to determine electronic excitation and ultraviolet-visible spectra. The oscillator strength and energy derived from TD-DFT closely match experimental results. Optimized geometries are obtained through constrained closed-shell formalism without symmetry restrictions. This study included the calculation of key properties such as ionization potential, electron affinity, chemical potential, negative electronegativity (χ), hardness, softness (S), electrophilicity index, and dipole moment (μ). The results indicate charge transfer within the molecule, and the molecular electrostatic potential (MESP) contour map highlights its electrophilic regions [11]. Koopmans' theorem uses the energy levels of the highest occupied molecular orbital (HOMO) and the lowest unoccupied molecular orbital (LUMO) to determine ionization potential (IP) and electron affinity (EA). According to Koopmans' theorem: $IP{=}{-}\varepsilon HOMO$ and $EA{=}{-}\varepsilon LUMO$ [12]. Each parameter is calculated as follows [13]:

(Electronegativity χ): $\chi = \frac{\mathrm{IP+EA}}{2}$ (1)

(Hardness): $\eta = \frac{\mathrm{IP-EA}}{2}$ (2)

(Softness) : $S = \frac{1}{\eta}$ (3)

(Electrophilic index): $\omega = \frac{-\chi^2}{2\eta}$ (4)

The dipole moment of a molecule is a crucial characteristic primarily employed to investigate nonbonded dipole-dipole interactions; a greater dipole moment is associated with more robust interactions between molecules [14].

3. RESULTS AND DISCUSSION

Figure 2 depicts the variations in wavelength recorded with UV technology within the spectrum of 300-800 nm. The electronic absorption spectra of PM 580 at λ max = 515 nm reveal the molecular orbitals' configuration in the initial electron transfer. This method reveals a significant absorption peak with an oscillator strength of 0.36, and these results are consistent with the experimental results of the researcher.

PM-580 exhibited a maximum absorption at approximately 500 nm, placing it in the middle of the spectrum in terms of absorption in the visible spectrum. Compared to PM-546, which has a λmax ≈ of 546 nm, PM-580 absorbs at a shorter wavelength. This decrease in λmax reflects a reduction in electronic stretching, giving PM-580 the ability to efficiently absorb the green light spectrum, without shifting toward red absorption as in PM-597 and PM-650. This enables its use in photodetection applications where absorption in the 480–520 nm range is preferred [15].

The nature of the solvent, particularly its polarity, significantly influences the position and intensity of the UV-Vis absorption spectra of organic dyes such as PM-580. In polar solvents, the excited state is typically more stable than the ground state, resulting in a bathochromic (red) shift in the absorption maximum (λmax). In contrast, nonpolar solvents may cause an under shift (blue) due to poor stability. Interactions such as hydrogen bonding can also broaden the absorption band and reduce peak intensity. Understanding these effects is essential for improving dye performance in sensing or laser applications [16].

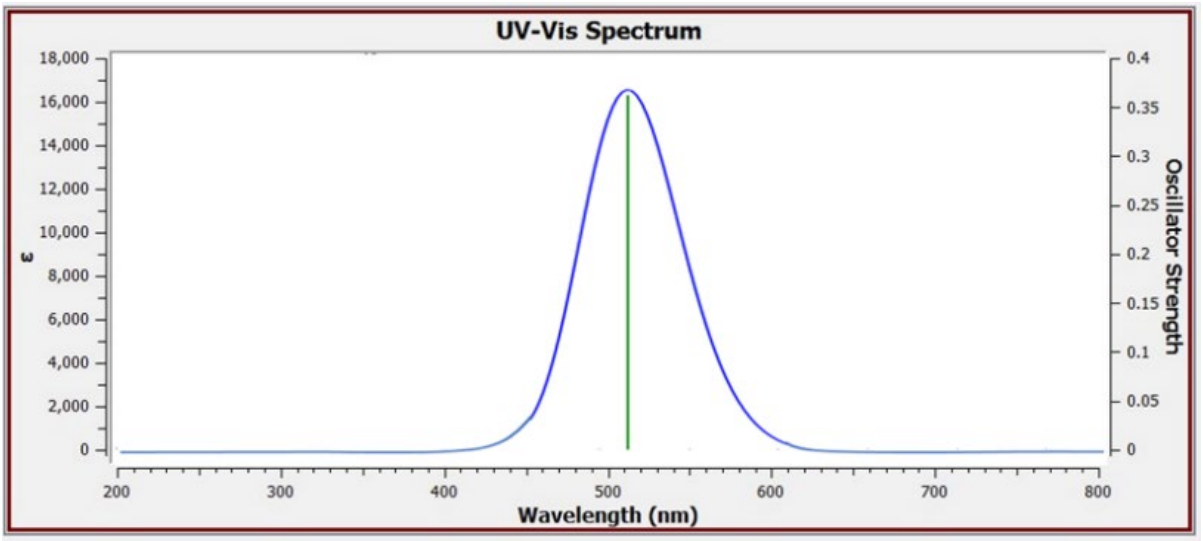

Figure 2 TD-B3LYP -UV spectrum of the PM 580.

Figure 3 show The absorption spectrum of pyrromethene 580 dye dissolved in ethanol solvent is measured at several different concentrations ($1x10^{-3}$, $5x10^{-4}$, $1x10^{-4}$, 5×10^{-5}, $1x10^{-5}$ and $1x10^{-6}$) M. Measurements of absorption spectra showed that the change in the concentration of (PM 580) affects the absorption spectra as shown in figure. In general, the intensity of absorbance increases with increasing the concentration of the dye in the solutions, the lowest concentration of $1x10^{-6}$ M exhibited the minimum intensity (0.37) at a wavelength of 520 nm, and the highest concentration $1x10^{-3}$ M, exhibited the maximum intensity (1.71) at wavelength 524 nm. It is clear from the above results that the peak of the absorption spectrum tends towards the shorter wavelength (blue shift) when decreasing the concentration. We also note that when the concentration increases, the intensity of absorbance increases.

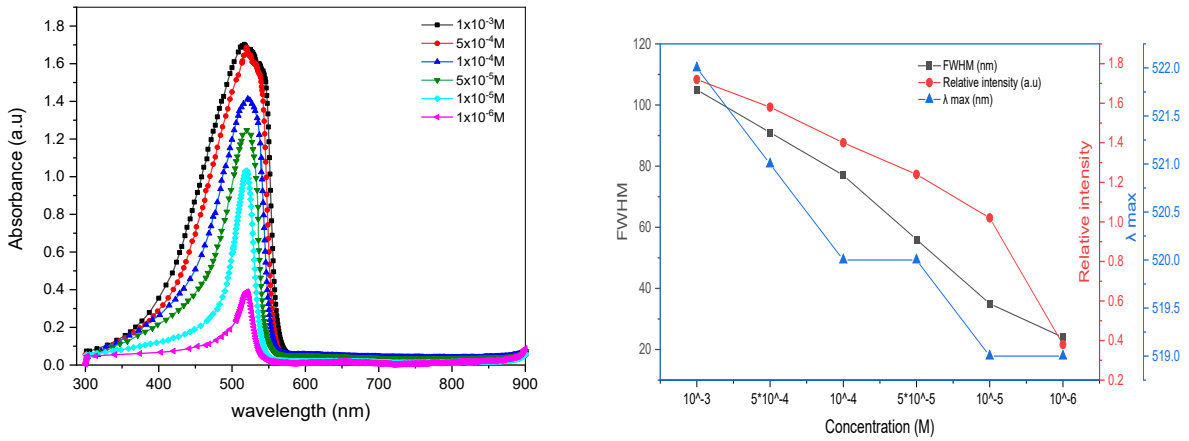

Figure 3 The absorption spectra of different molar concentrations of Pyrromethene 580.

Full width at half maximum (FWHM) an increase with increasing concentration, due to the increase in the number of molecules, which in turn leads to an increase in the absorption potential as shown in Table 1, and this absorption of dyes correspond to the law of Beer-Lambert, which states that the amount of absorbed light is proportional to the number of particles and concentration of the medium along the path. By comparing the results of the computer study with the practical results, we find that these results are consistent with each other.

Table 1 Absorption spectra and λ max and FWHM of Pyrromethene 580 dye at different concentrations.

Concentration (M)	***λ max*** **(nm)**	**FWHM (nm)**	**Relative intensity (abs) (a.u)**
1x 10^{-3}	522	105	1.72
5x10^{-4}	521	91	1.58
1x10^{-4}	520	77	1.40
5x10^{-5}	520	56	1.24
1x10^{-5}	519	35	1.02
1x10^{-6}	519	24	0.38

Figures 4 and 5 present the absorption and fluorescence spectra of PM-580 dissolved in ethanol after adding (Au: Ag) nanoparticles synthesized by laser ablation at different pulse energies (400–1000 mJ, 532 nm). The nanoparticles are introduced into dye solutions with a concentration of 1×10^{-6}M, while Table 2 summarizes the corresponding absorption maxima and FWHM values. The absorption intensity increases with increasing ablation energy, reaching a maximum at 1000 mJ, accompanied by spectral narrowing and a slight blue shift (~4 nm), which is attributed to enhanced photon trapping and improved nanoparticle dispersion within the dye solution.

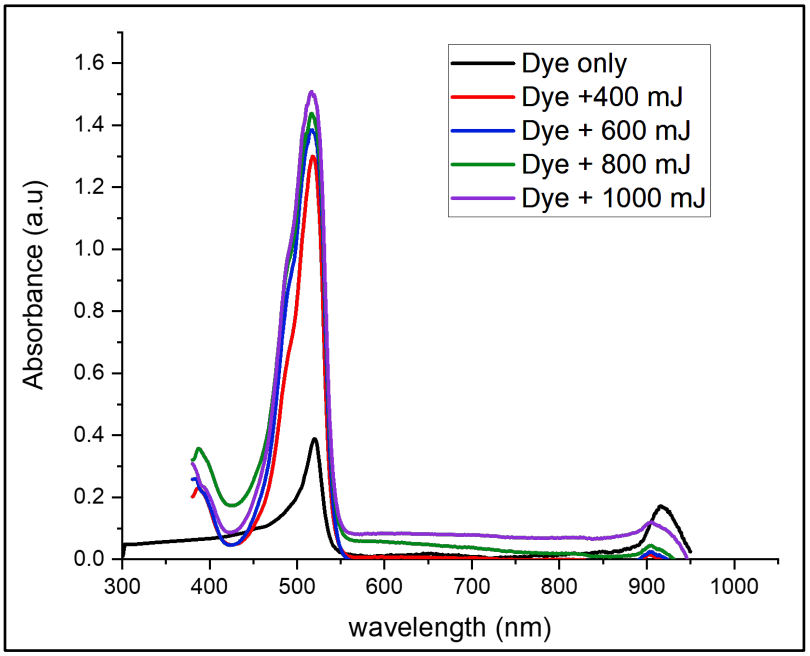

Figure 4 The Absorption spectra of 10^{-6} M molar concentration of PM 580 dye with (Au: Ag 532) NPs recorded at a different energy pulse.

Table 2 explain the values of intensity (Absorbance) and λmax, for 10^{-6} M of PM 580 dye with (Au: Ag) nanoparticles.

Energy pulses	**Laser wavelength (nm)**	**Au: Ag + Dye**		
		Abs	**λ_{max}**	**FWHM**
400	532	1.29	518	42
600		1.37	517	52
800		1.43	516	54
1000		1.50	516	54

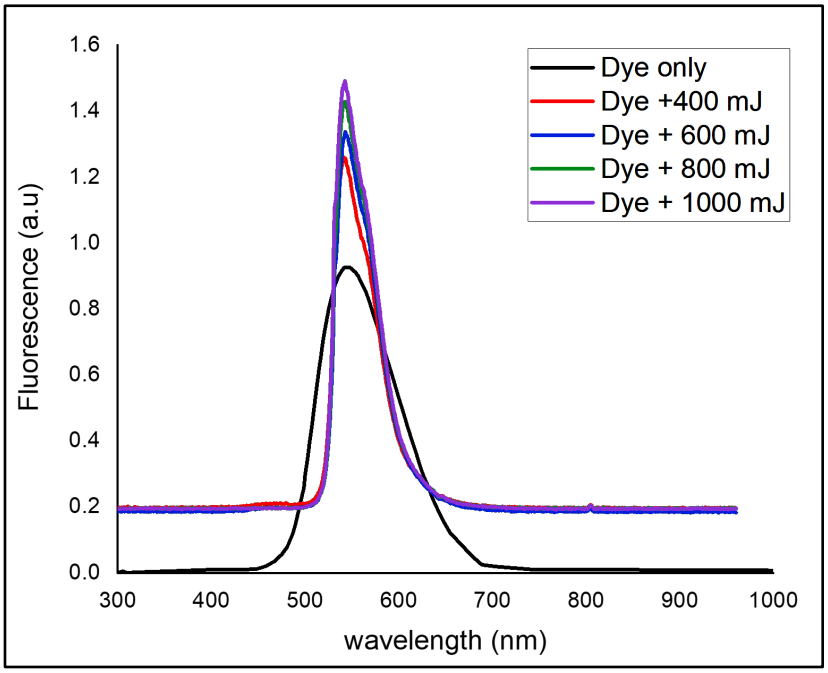

Figure 5 The fluorescence spectra of 10^{-6} M molar concentration of PM 580 dye with (Au: Ag 532) NPs recorded at a different energy.

3.1 Bond lengths

In molecular structure, bond separation, bond length, or internuclear distance refers to the standard distance between the nuclei of two atoms bonded within a molecule. It is a characteristic of the atomic bond that can be transferred. Bond length has an inverse relationship with bond order; bond length decreases as the number of electrons involved in bond formation increases. Conversely, bond length is inversely related to bond strength and dissociation energy. A stronger overall relationship, considering all contributing factors, results in a shorter bond length. Bond lengths are measured in angstroms (1 Å = 10^{-10} meters) or picometers (1 pm = 10^{-12} meters). Table 3 shows the selected bond lengths (Å) of PM580, determined using B3LYP methods, as illustrated in Figure 6 [17].

Table 3 Selected bond lengths (Å) of PM580, determined using B3LYP methods.

Table 3 Code	Assignment	Value (Å)	Code	Assignment	Value (Å)
R1	N1-B2	1.554	**R32**	C17-H26	1.0944
R2	N1-C4	1.3962	**R33**	C18-H27	1.0946
R3	N1-C8	1.3469	**R34**	C18-H28	1.0971
R4	B2-N3	1.5547	**R35**	C18-H29	1.0917
R5	B2-F14	1.3947	**R36**	C19-H30	1.0921
R6	B2-F15	1.3956	**R37**	C19-H31	1.0972
R7	N3-C5	1.3968	**R38**	C19-H32	1.0943
R8	N3-C7	1.3455	**R39**	C20-H34	1.0907
R9	C4-C6	1.4095	**R40**	C20-H35	1.0937
R10	C4=C9	1.4338	**R41**	C20-H36	1.0943
R11	C5=C6	1.4083	**R42**	C38-H39	1.0984
R12	C5-C10	1.4354	**R43**	C38-H40	1.0982
R13	C6-C16	1.5085	**R44**	C38-C41	1.5331
R14	C7=C11	1.4176	**R45**	C41-H42	1.0988
R15	C7-C17	1.4946	**R46**	C41-H43	1.0986
R16	C8=C12	1.4176	**R47**	C41-C44	1.5315
R17	C8-C20	1.4950	**R48**	C44-H45	1.0948
R18	C9-C12	1.4003	**R49**	C44-H46	1.0959
R19	C9-C18	1.5026	**R50**	C44-H47	1.0958
R20	C10-C11	1.3986	**R51**	C48-H49	1.0967
R21	C10-C19	1.5025	**R52**	C48-H50	1.0965
R22	C11-C13	1.5050	**R53**	C48-C51	1.5463
R23	C12-C48	1.5071	**R54**	C51-H52	1.0984
R24	C13-H36	1.0968	**R55**	C51-H53	1.0987
R25	C13-H37	1.0973	**R56**	C51-C54	1.5327
R26	C13-C38	1.5424	**R57**	C54-H55	1.0968
R27	C16-H21	1.0871	**R58**	C54-H56	1.0986
R28	C16-H22	1.0875	**R59**	C54-C57	1.5317
R29	C16-H23	1.0976	**R60**	C57-H58	1.0948
R30	C17-H24	1.0938	**R61**	C57-H59	1.0960
R31	C17-H25	1.0912	**R62**	C57-H60	1.0961

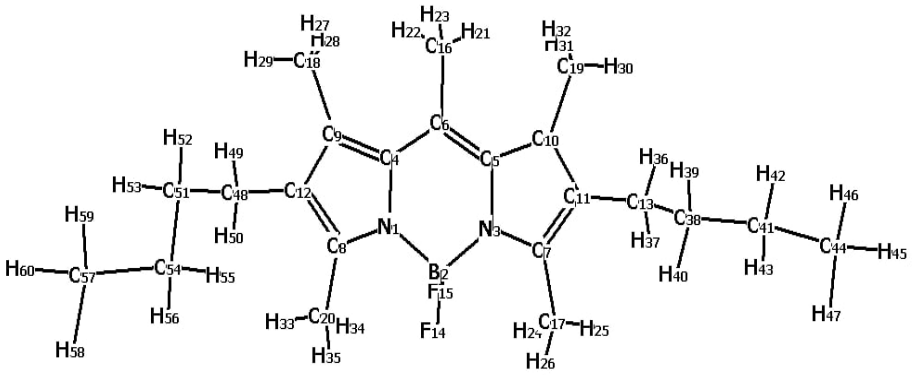

Figure 6 Optimized geometric structure of the bond length PM580 by B3LYP.

3.2 Angles of bond

The angle separating two bonds that possess a shared atom, usually measured in degrees. The calculated bond angles obtained using DFT methods are displayed in Table 4.

Table 4 Selected bond angles (degrees) for PM580.

Code	Assignment	Value	Code	Assignment	Value
A1	B2-F14	126.0748	**A60**	C9-C18-H29	110.3819
A2	B2-N1-C8	124.8466	**A61**	H27-C18-H28	107.181
A3	C4-N1-C8	109.07	**A62**	H27-C18-H29	107.238
A4	N1-B2-N3	106.1214	**A63**	H28-C18-H29	106.8725
A5	N1-B2-F14	109.9479	**A64**	C10-C19-H30	110.3379
A6	N1-B2-F15	110.3256	**A65**	C10-C19-H31	112.5035
A7	A(3,2,14)	109.8496	**A66**	C10-C19-H32	112.36
A8	N3-B2-F15	110.205	**A67**	H30-C19-H31	106.8915
A9	F14-B2-F15	110.3095	**A68**	H30-C19-H32	107.1925
A10	B2-N3-C5	126.1243	**A69**	H31-C19-H32	107.2515
A11	B2-N3-C7	124.8222	**A70**	C8-C20-H33	111.2692
A12	C5-N3-C7	109.0426	**A71**	C8-C20-H34	110.0408
A13	N1-C4-C6	120.3731	**A72**	C8-C20-H35	110.5267
A14	N1-C4=C9	107.3435	**A73**	H33-C8-H34	109.3034
A15	C6-C4=C9	132.276	**A74**	H33-C20-H35	108.9313
A16	N3-C5=C6	120.304	**A75**	H34-C20-H35	106.6486
A17	N3-C5-C10	107.3316	**A76**	C13-C38-H39	109.1528
A18	C6=C5-C10	132.3595	**A77**	C13-C38-H40	109.1351
A19	C4-C6=C5	120.7015	**A78**	C13-C38-C41	113.2032
A20	C4-C6-C16	119.577	**A79**	H39-C38-C41	105.8258
A21	C5=C6-C16	119.721	**A80**	H39-C38-C41	109.6365
A22	N3-C7=C11	109.5967	**A81**	H40-C38-C41	109.6205
A23	N3-C7-C17	121.7253	**A82**	C38-C41-H42	109.2462
A24	C11=C7-C17	128.678	**A83**	C38-C41-H43	109.2206
A25	N1-C8=C12	109.5665	**A84**	C38-C41-C44	113.2292
A26	N1-C8-C20	121.3729	**A85**	H42-C41-H43	105.9208
A27	C12=C8-C20	129.0582	**A86**	H42-C41-C44	109.4692
A28	C4=C9-C12	106.9777	**A87**	H43-C41-C44	109.4938
A29	C4=C9-C18	128.8587	**A88**	C41-C44-H45	111.4506
A30	C12-C9-C18	124.1595	**A89**	C41-C44-H46	111.199
A31	C5-C10-C11	106.9043	**A90**	C41-C44-H47	111.2194
A32	C5-C10-C19	128.8604	**A91**	H45-C44-H46	107.6593
A33	C11-C10-C19	124.2177	**A92**	H45-C44-H47	107.6577
A34	C7=C11-C10	107.1205	**A93**	H46-C44-H47	107.4618
A35	C7=C11-C13	125.2251	**A94**	C12-C48-H49	109.3303
A36	C10-C11-C13	127.637	**A95**	C12-C48-H50	109.455
A37	C8=C12-C9	107.0368	**A96**	C12-C48-C51	115.1181
A38	C=C12-C48	126.0815	**A97**	H49-C48-H50	105.3593
A39	C9-C12-C48	126.8809	**A98**	H49-C48-C51	108.4692
A40	C11-C13-H36	109.8647	**A99**	H50-C48-C51	108.6564
A41	C11-C13-H37	109.4652	**A100**	C48-C51-H52	109.222

A42	C11-C13-C38	114.0632	**A101**	C48-C51-H53	108.3656
A43	H36-C13-H37	105.3305	**A102**	C48-C51-C54	114.5579
A44	H36-C13-C38	108.9832	**A103**	H52-C51-H53	106.183
A45	H37-C13-C38	108.7628	**A104**	H52-C51-C54	109.0637
A46	C6-C16-H21	111.4742	**A105**	H53-C51-C54	109.1172
A47	C6-C16-H22	111.3144	**A106**	C51-C54-H55	109.4066
A48	C6-C16-H23	111.3131	**A107**	C51-C54-H56	109.2164
A49	H21-C16-H22	107.4448	**A108**	C51-C54-H57	112.9138
A50	H21-C16-H23	107.586	**A109**	H55-C54-H56	106.2104
A51	H22-C16-H23	107.5005	**A110**	H55-C54-C57	109.5021
A52	C7-C17-H24	110.1741	**A111**	H56-C54-C57	109.3698
A53	C7-C17-H25	111.1626	**A112**	C54-C57-H58	111.4152
A54	C7-C17-H26	110.4648	**A113**	C54-C57-H59	111.1931
A55	H24-C17-H25	109.2726	**A114**	C54-C57-H60	111.2948
A56	H24-C17-H26	106.6008	**A115**	H58-C57-H59	107.6032
A57	H25-C17-H26	109.0482	**A116**	H58-C57-H60	107.6585
A58	C9-C18-H27	112.4859	**A117**	H59-C57-H60	107.4811
A59	C9-C18-H28	112.3757			

3.3 Electronic properties

The highest occupied molecular orbital (HOMO) primarily serves as an electron donor, whereas the lowest unoccupied molecular orbital (LUMO) predominantly acts as an electron acceptor. Their eigenvalues, along with their energy gap, indicate the chemical reactivity of the molecule [18]. Figure 7 depicts the 3-dimensional electrostatic potential maps of PM-580. Regions displaying negative electrostatic potential are vulnerable to electrophilic assault [19,20]. A reduced energy gap between them signifies that electron in HOMO can be more easily excited. Elevated HOMO energies indicate a greater capacity for electron donation, whereas reduced LUMO values signify an enhanced capacity for electron acceptance, as shown in Fig 4. PM-580 dye exhibited an electron energy gap (Eg) of 2.99 eV, which is higher than that of PM-597 (2.2 eV), indicating higher electronic stability and lower photoexcitability at long wavelengths [21] Also, it exhibited a relatively low HOMO value (-5.18 eV) compared to PM-650 dye (-4.9 eV), reflecting a higher resistance to photooxidation processes and enhancing the dye's stability in strong light environments [22]. On the other hand, the LUMO energy of PM-580 dye is -2.22 eV, which is higher than the LUMO of PM-597 (~ -2.8 eV), which reduces its ability to gain electrons and limits reduction reactions, which contributes to enhancing the chemical stability of the compound [23]. Table 4 displays the overall energy values, electronic states for the examined structure, the energy gap, and the dipole moment (μ) of PM-580. The experimentally determined ground-state dipole moment is 3.961364 Debye [24]. The B3LYP functional used in this study is particularly effective for determining the electronic properties of the examined organic compounds, including ionization potentials (IP), electron affinities (EA), chemical potential (K), absolute hardness (η), absolute softness (S), and electrophilic index (ω) as shown in Table 5.

Table 5 Electronic properties of PM-580.

Property	TD-DFT B3LYP/6-31G (d,p)
IP (eV)	5.18008
EA (eV)	2.21968
χ (eV)	3.69988
ω(eV)	4.62407513
ε(eV^{-1})	0.216259462
η (eV)	1.4802
S (eV^{-1})	0.67558438
C_p (eV)	-3.69988
Etot (a.u.)	-1192.534269
E_{HOMO} (eV)	-5.18008
E_{LUMO} (eV)	-2.21968
E_{Gap}(eV)	2.960393 eV

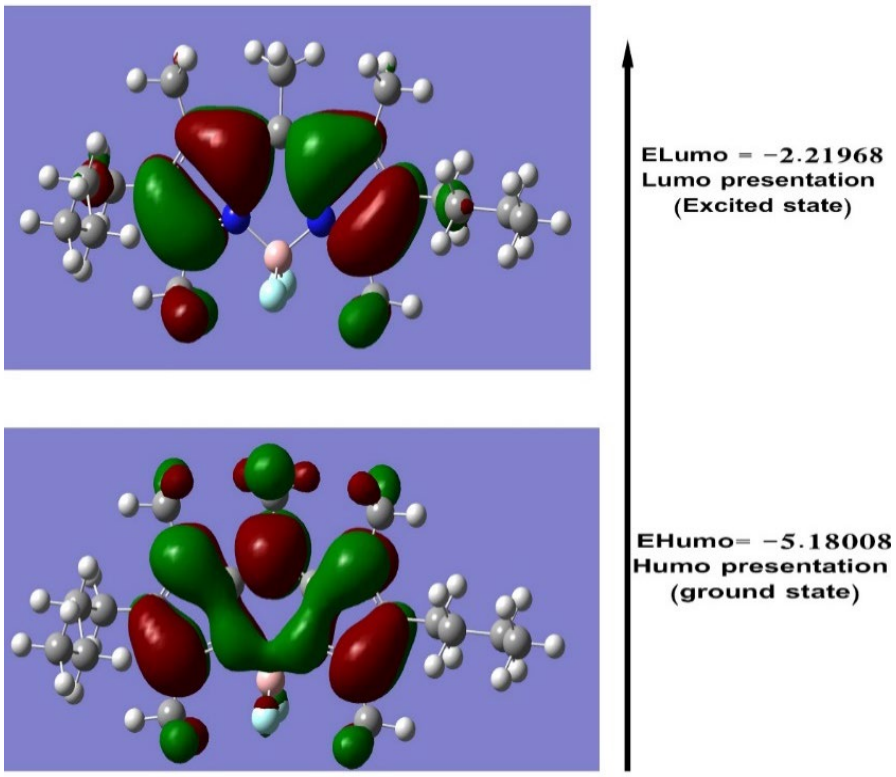

Figure 7 Optimized geometric structure of the bond length PM580.

3.4 Molecular potential distribution (MEP)

The molecular electrostatic potential (MEP) at a specific site near a molecule indicates the overall electrostatic effect from the molecule's full charge distribution of electrons and nuclei at that point. This potential is related to dipole moments, electronegativity, partial charges, and the chemical reactivity of molecules. Understanding charge distributions aids in explaining molecular interactions, while recognizing electrostatic potential can identify a molecule's reactive regions [25].

Figure 8 depicts the 3-dimensional electrostatic potential patterns of PM-580. Regions displaying negative electrostatic potential are vulnerable to electrophilic assault. In the ESP map, red areas represent regions of negative potential (electron-rich), blue regions represent positive potential (electron-deficient), and green regions represent neutral electrostatic potential [26,27].

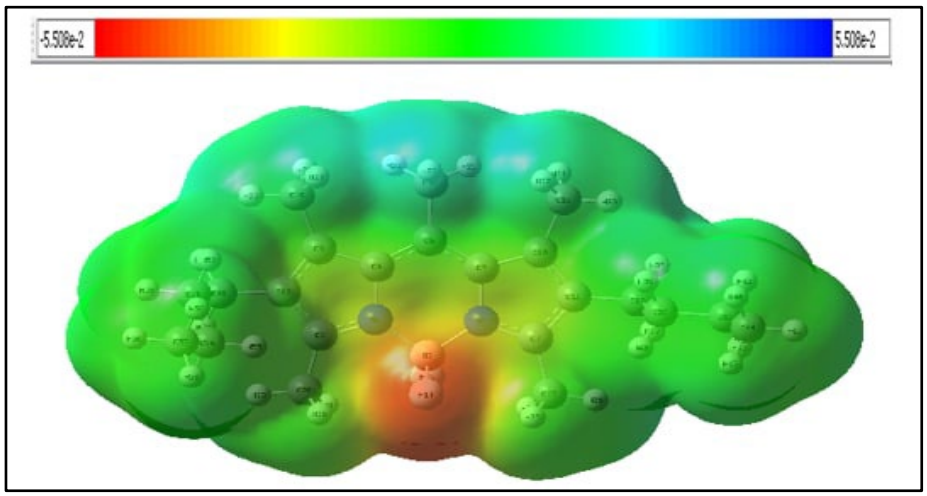

Figure 8 Molecular electrostatic potential mapped onto a surface of total electron density for PM-580.

4. CONCLUSIONS

This work examines the configuration and electronic characteristics spectra of Pyrromethene 580 utilizing (DFT/TDDFT) methodologies while accounting for the solvent effect on the absorption spectra. The results indicate that TDDFT is a proficient method for examining the spectra and excited-state properties of Pyrromethene 580. Oscillator strength, absorption (max wavelength) λ_{max}, and excitation energies of the molecule were ascertained using TDDFT methods and compared with experimental data, demonstrating significant concordance.

References

[1] J. Siesicki, Synthesis and Characterisation of Mono-and Bi-dentate BODIPY Based Chromophores for CdSe Containing Hybrid Nanomaterials, Te Herenga Waka-Victoria University of Wellington, 2025 https://doi.org/10.26686/wgtn.28516922
[2] L.R. Morgan, A. Chaudhuri, L.E. Gillen, J.H. Boyer, L.T. Wolford, Photodynamic Therapy: Mechanisms II, SPIE (1990) 253–265 https://doi.org/10.1117/12.17671
[3] Haneen Khaled Naji Al-Samarrai, Osama Nadhom Nijris, Mohammed Fadhil AboKsou, Exp. Theo. NANOTECHNOLOGY 9 (2025) 529 https://doi.org/10.56053/9.4.529

[4] Maksood Adil Mahmoud Al-Doori, Nahedh Ayad Faris, Noor Adnan Mahmood, Asaad T. Al-Douri, Luay Mannaa ibrahim, Amna M. Al-Tikrity, Exp. Theo. NANOTECHNOLOGY 9 (2025) 555 https://doi.org/10.56053/9.4.555
[5] Asaad T. Al-Douri, Alaa A. Khaleel, Luay Mannaa ibrahim, Abeer Talib Abdulqader, Ammr Khalid Shihab, Mustafa Khaleel Ibrahim, Maksood Adil Mahmoud Al-Doori, Exp. Theo. NANOTECHNOLOGY 9 (2025) 563 https://doi.org/10.56053/9.4.563
[6] F. Furche, D. Rappoport, Theor. Comput. Chem. 16 (2005) 93–128 https://doi.org/10.1016/S1380-7323(05)80020-2
[7] S.B. Mohammed, N.T. Latif, T.M. Talib, A.S. Sameer, S.M. Obaid, F.A. Majeed, High Energy Density Phys. (2025) 101240 https://doi.org/10.1016/j.hedp.2025.101240
[8] M.H. Suhail, Z.A. Al Shadidi, Q. Hammad, S.N. Kareem, Exp. Theo. Nanotechnology (2025) 273–286 https://doi.org/10.56053/9.S.273
[9] S.B. Mohammed, H.A. Yıldırım, Russ. J. Phys. Chem. A 520 (2025) 140–149 https://doi.org/10.1134/S0012501625600858
[10] Hayder Subhi FAISAL, Cezar Mohamed Ahmed, Ayaa Ayad abeed, Mais Qasem Mohammed, Asaad T. Al-Douri, Semaa Amer Ghanam, Zeena T. Khattab, Aya Abdullateef Ezat, Maksood Adil Mahmoud Al-Doori, Nida Muhsin Ali, Mohammed Ameri, Mohammad Mutlag Salih, Exp. Theo. NANOTECHNOLOGY 9 (2025) 571 https://doi.org/10.56053/9.4.571
[11] Björn Reetz, Andreas Frehn, Wolfgang Budweiser, William Bishop, Exp. Theo. NANOTECHNOLOGY 9 (2025) 465 https://doi.org/10.56053/9.3.465
[12] C. Lee, W. Yang, R.G. Parr, Phys. Rev. B 37 (1988) 785 https://doi.org/10.1103/PhysRevB.37.785
[13] F.A.H. Mutlak, A.T. Mohi, T.J. Alwan, Baghdad Sci. J. 13 (2016) 143 https://doi.org/10.21123/bsj.2016.13.2.2NCC.0143
[14] S.R. Kumar, N. Vijay, K. Amarendra, P. Onkar, S. Leena, Res. J. Recent Sci. (2012)
[15] T.R. Al-Biladi, A.S. Al Dwayyan, M.N. Khan, S.M.H. Qaid, K. Al Zahrani, J. Spectrosc. (2015) 901032 https://doi.org/10.1155/2015/901032
[16] Maksood Adil Mahmoud Al-Doori, Asaad T. Al-Douri, Nahedh Ayad Faris, Exp. Theo. NANOTECHNOLOGY 9 (2025) 489 https://doi.org/10.56053/9.3.489
[17] N.K. Rasheed, A.N. Ayaash, Iraqi J. Sci. (2021) 2536–2542 https://doi.org/10.24996/ijs.2021.62.8.6
[18] Ahmed Suhail Hussein, Younis W. Younis, Saeb Jasim Mohammed Alnajm, Shaimaa Tarik Mahmood, Sama Amer Abbas El-Tekreti, Mais Qasem Mohammed, Mais Qasem Mohammed, Ali Y. Alwan, Abbas Saeb Zaham, Asaad T. Al-Douri, Noor Khalid Ismael, Maksood Adil Mahmoud Al-Doori, Exp. Theo. NANOTECHNOLOGY 9 (2025) 505 https://doi.org/10.56053/9.3.505
[19] Saad Ahmed Alnuaimi, D. Vaishnavi, Huda Ghazi Hameed, Exp. Theo. NANOTECHNOLOGY 9 (2025) 513 https://doi.org/10.56053/9.3.513
[20] A. Tony, R. Clarison, Exp. Theo. NANOTECHNOLOGY 9 (2025) 347 https://doi.org/10.56053/9.2.347
[21] Safa Salah Salman, Asaad T. Al-Douri, Albosale Abbas Hadi, Saeb Jasim Mohammed Alnajm, Exp. Theo. NANOTECHNOLOGY 9 (2025) 361 https://doi.org/10.56053/9.2.361
[22] J. Belić, A. Förster, J.P. Menzel, F. Buda, L. Visscher, Phys. Chem. Chem. Phys. 25 (2023) 19266–19268 https://doi.org/10.1039/D1CP04218A
[23] M. Sadeldine, Exp. Theo. NANOTECHNOLOGY 9 (2025) 1 https://doi.org/10.56053/9.1.1
[24] D. Glossman-Mitnik, J. Mol. Struct. THEOCHEM 911 (2009) 105–108 https://doi.org/10.1016/j.theochem.2009.07.006
[25] N. M. Slaber, J. S. Kith, Exp. Theo. NANOTECHNOLOGY 9 (2025) 9 https://doi.org/10.56053/9.1.9
[26] Badis Bendjemil, Maram Mechi, Khaoula Safi, Mounir Ferhi, Karima Horchani Naifer, Exp. Theo. NANOTECHNOLOGY 8(2024) 51 https://doi.org/10.56053/8.3.51
[27] X.K. Chen et al., Org. Electron. 12 (2011) 1198–1210 https://doi.org/10.1016/j.orgel.2011.03.029

Exp. Theo. NANOTECHNOLOGY 10 (2026) 357-371